Multiple Photonic Bound States in the Continuum in an Electromagnetically Induced Transparency Metasurface

Yaolin Hu ⓘ, Suxia Xie ⓘ, Chongjun Bai ⓘ, Weiwei Shen ⓘ, and Jingcheng Yang

Abstract—Bound state in the continuum (BIC), as a novel eigen-mode with infinitely high-quality factor, has received great attention in modern optical science. Mode coupling in dielectric metasurfaces opens possibilities in searching for robust BICs. Here, we discover multiple BICs in periodic dielectric resonators composed of a silicon rectangular bar and a silicon ring in one lattice. For the symmetry-protected BIC at-Γ point, a sharp electromagnetically induced transparency window can be formed by either tilting incident angle to induce the 'bright-bright' mode coupling, or by displacing the ring to generate the 'bright-dark' mode coupling. Besides, the coupling between two resonators leads to a new energy band in the dielectric metasurface. As a result, two off-Γ BICs are formed owing to avoided crossings with two energy bands, and another one belongs to the single-resonance parametric BIC. Thus, our coupled resonators possess superior abilities to judiciously engineer BICs via versatile physical mechanisms. Taking advantage exclusively of coupled resonators in dielectric metasurfaces provides fresh insights into the creation of both symmetry-protected and accidental BICs, which enables profound advancements in designing novel photonic devices.

Index Terms—Bound states in the continuum, electromagnetically induced transparency, metasurface, Q-factor.

I. INTRODUCTION

AS ONE of the nonradiating electromagnetic states, bound state in the continuum (BICs) has received great attention for light trapping since the leakage rate is significantly reduced to zero when photons are perfectly trapped [1], [2]. Such a strongly confined state, originally proposed by J. von Neumann

Yaolin Hu is with the School of Physics and Electronic Science, Hunan University of Science and Technology, Xiangtan 411199, China (e-mail: hyl_yaolin@sina.com).

Suxia Xie was with the School of Physics and Electronic Science, Hunan University of Science and Technology, Xiangtan 411199, China. She is now with the School of Mechanical Engineering, University of Shanghai for Science and Technology, Shanghai 200093, China (e-mail: xsx@usst.edu.cn).

Chongjun Bai, Weiwei Shen, and Jingcheng Yang are with the School of Mechanical Engineering, University of Shanghai for Science and Technology, Shanghai 200093, China (e-mail: 1793434598@qq.com; 1050168529@qq.com; yjccccc@outlook.com).

and E. Wigner in the context of quantum mechanics [3], [4], is typically formed through destructive interference between two or more leaky modes. By tuning the structure symmetry [5] or the coupling strength between different resonance channels [6], [7], quasi-BICs are generated with a ultranarrow linewidth. Such associated high-Q resonances around a BIC point have earned considerable attention to construct ultra-sharp transmission/reflection spectra, leading to a giant near-field enhancement and various promising applications, such as BIC-based chirality [8]–[11], lasing [12]–[14] beam shifting [15], [16], decreasing radiative losses [17], nonlinearity [18]–[22], modulation [23], [24] and sensing [25]. In photonic systems, one case is symmetry-protected BICs located at the center of Brillouin zone (Γ point), which is relevant to the complete incompatibility between resonant mode and radiative channels due to symmetry mismatch [5], [26]. Another type of BICs emerging at accidental in-plane wavevectors (off-Γ points) are known as accidental or resonance-trapped BICs [27], [28]. Accidental BICs are usually excited by destructive interferences between isolated resonances [29], [30]. Over the last decade, much research has examined the transformation from ideal BIC into leaky quasi-BICs by fine-breaking structural symmetry or varying angle of incidence [31]–[35].

Compared with the metallic counterparts, dielectric metasurfaces have ignited interest in the exploration of BICs because dielectric material can largely avoid the intrinsic Ohmic loss for extremely high Q generation [36], [37]. In a manner analogous to electronic band structures, it is also a driving force behind recent advances that the dispersion and spectral features of dielectric metasurfaces can be engineered to support BICs [38]. In addition to the geometric symmetry design, the guided modes supported by a dielectric metasurface can form multiple isolated bands, which provides another degree of freedom to create off-Γ BICs [39]–[41]. Various structures in dielectric metasurfaces have been proposed and studied for countless applications in radiation modulation [42], biosensing [43]–[45], refractometric sensing [46], and polarization tailoring [47]–[49]. By introducing external perturbations in dielectric metasurfaces, the quasi-BICs leak as Fano resonances exhibiting narrow far-field lineshapes, offering a new avenue for strong localization of near-field electromagnetic energy. To realize an ideal BIC, the coupling between different modes is always adopted as a feasible route. Consequently, several structures have been proposed

and verified either experimentally or numerically [50]–[57]. As a special case of resonance resulted from dual modes interactions, electromagnetically induced transparency (EIT) takes place when the frequencies of strongly and weakly damped oscillators exactly match [58]. This effect has also shown great promise in developing novel devices, such as slow light photonic devices [59], on-chip buffers [60], sensitive sensors [61], and electromagnetically induced modulators [62]. More recently, few works have realized the EIT effect by transforming the BIC point into quasi-BIC state, thus indicating some intrinsic connections between the BIC and EIT phenomena [63]–[65]. Notably, by employing the interaction between dark and bright modes based on silicon rectangular bars and rings, EIT-resonant metasurfaces with high quality factors Q > 400 have been demonstrated experimentally [66]. A highly efficient visible third harmonic generation and all-optical nonlinear modulation have then been verified in this EIT system [67]. These experimental data have revealed great application value of the coupled dielectric resonators in nanophotonics. Unfortunately, the underlining physical origin has been simply regarded as the analogy of 3-level Fano-resonant system, understanding on the BIC nature of such type in-plane coupled dielectric resonators is still relatively scarce. Novel insights into the ultra-high-quality-factor resonances in this system are highly desired due to both curiosities in fundamental physics and demands in technological applications.

In this work, multiple BICs are discovered in an array of periodic nano resonators combined a silicon rectangle bar and a silicon ring in one lattice. A comprehensive analysis reveals the existence of both symmetry-protected BICs and accidental BICs due to the coupling effect between two resonators. For the symmetry-protected BIC at-Γ point, the dipole moment of rectangular bars plays the role of continuum as a broadband resonance dip. A leakage channel in the form of a sharp radiating EIT window is invoked by two mechanisms. One is the 'bright-bright' mode coupling via the incident angle tilting, and another is the 'bright-dark' mode coupling through the in-plane mirror symmetry breaking. Owing to a new energy band formed by the two resonators' coupling, three off-Γ BICs are created in this system when the incident angles are 17.6°, 36.1° or 47.9°, respectively. Two of them are ascribed to the avoided crossings with two energy bands and another one belongs to the single-resonance parametric BIC. Moreover, the radiative Q-factors of all quasi-BICs can reach up to 10^5 and tend to infinity at discrete points. They also obey an inverse square dependence on the structural asymmetry or the in-plane wave vector deviation. The observations not only directly manifest the inner connection between EIT effect and quasi-BIC state in the proposed dielectric resonators, but also offers unique possibilities in searching for multiple BICs.

II. RESULTS AND DISCUSSION

To reveal the role of coupling for the excitation of BICs in dielectric metasurface, we propose coupled resonators consisting of a rectangular bar and a ring within one unit-cell. By considering the dispersionless feature in the spectral region of interest,
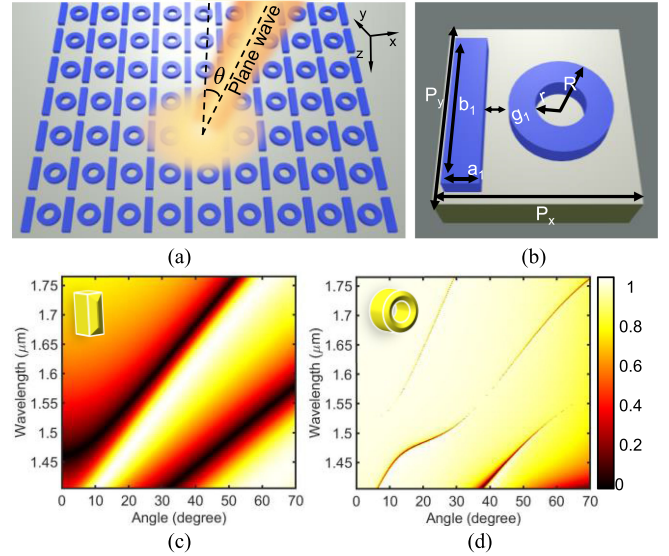

Fig. 1. (a) Overall diagram of the metasurface. The geometrical structure is composed of all-dielectric silicon resonators and silica substrate. (b) Schematic of one unit-cell consisting of two coupled resonators. The geometrical parameters of the structure are: P_x = 920 nm, P_y = 960 nm, a_1 = 250 nm, b_1 = 920 nm, r = 120 nm, R = 260 nm, and the thickness of the silicon is 121 nm. Calculated transmission spectra of (c) periodic rectangular bars and (d) periodic rings in the wavelength ranging from 1.40 μm to 1.76 μm and the incident angle ranging from 0 ° to 70 °.

the structure is made of silicon whose refractive index is 3.7, and quartz is selected as the substrate with refractive index 1.48 according to the experimental work in [66]. The working principle is illustrated in Fig. 1(a). To investigate the symmetry-protected BIC, a plane wave polarized along y-direction is adopted as the normal incidence that propagates along z-direction. As for accidental BICs at off-Γ points, the plane wave is obliquely incident on the metasurface with an incident angle θ. Specifically, the silicon building blocks is graphically demonstrated in Fig. 1(b). In the picture of electromagnetically induced transparency (EIT), the rectangular bar and ring resonators serve as 'bright' and 'dark' modes, respectively [66]. The ring cannot be excited without the near-field coupling from the rectangular bar. In order to obtain a EIT transparent window centered at the dipole resonance frequency, the geometrical parameters are optimized as follows: the length and width of the bar are $b_1 = 920\ nm$ and $a_1 = 250\ nm$, respectively. The outer and inner radius of the ring are $R = 260\ nm$ and $r = 120\ nm$, respectively. The thickness of the silicon is fixed as 121 nm. To ensure an enough coupling strength, the periods are $P_x = 920\ nm$, $P_y = 960\ nm$, so that the spacing between two resonators is 75 nm. With the help of the CST Microwave Studio, we can systematically calculate transmission spectra, Q-factors, and near-field distributions by varying parameters such as the incident light angle (θ) and the spacing (g_1).

Before a comprehensive interpretation of the coupling-induced BICs, we here intuitively investigate the spectral responses of the bar and the ring separately by sweeping the angle of incidence, as shown in Fig. 1(c) and 1(d). At normal incidence of $\theta = 0°$, a resonant dip with a relative low Q-factor is observed around 1.46 μm. This phenomenon is ascribed to the collective
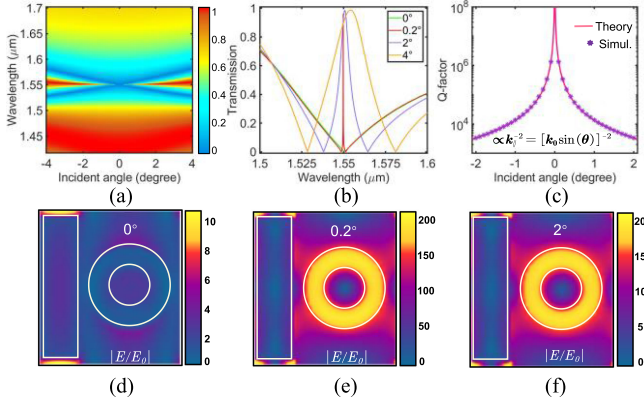
Fig. 2. (a) Calculated transmission spectra of the collective dark and bright modes in the wavelength ranging from 1.43 μm to 1.72 μm and in the incident angle ranging from -4° to 4°. (b) Calculated transmission spectra of the collective dark and bright modes in the wavelength ranging from 1.5 μm to 1.6 μm when the selected incident angles are: 0°, 0.2°, 2° and 4°. (c) Variation of Q factor of the collective dark and bright modes with varying incident angle. (d)-(f) Near-filed distributions at the function of incident angle at the x-y cross section at z = 60.5 nm when the corresponding wavelength is 1.55 μm.

oscillation of the bar resonator because the 'bright' mode can efficiently couple with the incoming wave. As the excitation light incident angle increases, the working frequencies of the modes in the rectangular bar all undergo an obvious redshift [40], [68]. Such an angle dependent dispersion would play an important role in realizing off-Γ BICs. When only one ring is considered, no resonant feature is obtained at normal incidence because the 'dark' magnetic dipole cannot be excited directly. However, one sharp resonant dip occurs with the increment of incident angle, indicating the so-called 'dark' mode is an at-Γ BIC point. The disappearance of linewidths at $\theta = 37°$ and $65°$ represents single-resonance parametric BICs which have been widely studied in dielectric metasurfaces [69]–[72]. Therefore, both individual resonators possess eigenmodes and specific angle-dependent dispersions in the spectral range of interest, laying a solid foundation for the investigation of BICs when two resonators are coupled with each other. In the following sections, we will conduct deeper investigations for the coupling-induced at-Γ BIC and off-Γ BICs, respectively.

A. Symmetry-Protected BICs at Γ Points

To gain further insight into the influence of the coupling, we first inspect the symmetry-protected BIC at-Γ point. As shown in Fig. 1(b), the system exhibits a typical in-plane mirror symmetry σ_x when $g_1 = 75\,nm$. The transmission spectrum of $\theta = 0°$ can be seen in Fig. 2(a) and 2(b) with no appreciable change when compared with the case of only one rectangular bar shown in Fig. 1(c). This means that the magnetic dipole mode in the ring is not excited and only the bright mode bar resonator couple to the far-field with a high radiative loss. The near electrical field distribution in Fig. 2(c) can be utilized to validate this physical mechanism where the near-field enhancement is observed merely around the rectangular bar gap. Since the periodicity is in the x and y directions, the resonance mode is no longer protected

by in-plane σ_x when the photonic state is away from the Γ point. Here, the 'σ_x' means an object has a mirror symmetry with a mirror plane that is perpendicular to the x-axis. By closely studying the incident angle-resolved transmission map, it is visible in Fig. 2(a) that a sharp transmission peak takes place. Such a sharp transparent window existing at the dip of resonance can also be considered as EIT effect. The result indicates that an ideal BIC can be obtained at 0° incident angle and the EIT effect is the at-Γ quasi-BIC. Please note the out-of-plane magnetic dipole mode in the ring opens a leakage channel to the far field when the incidence is not in the normal direction, as shown in Fig. 1(d). As a result, the destructive interference between magnetic dipole and electric dipole leads to a transparent window approaching to unity. The eigenmode analysis of the proposed structure is carried out by the software of COMSOL Multiphysics. In this way, the specific lineshape need not to be considered and the Q factor is $Q = Re(f_{eig})/2Im(f_{eig})$. The extracted Q-factors of the quasi-BIC are shown in Fig. 2(c). The ultra-high Q-factor can be more than 10^6 and decays quadratically ($Q \propto 1/k_{//}^2 \propto 1/|ksin(\theta)|^2$) with respect to the in-plane wavevectors. Q-factor tends to infinity at Γ point also indicates an ideal BIC at the electric dipole resonance dip. BIC is a new approach to trap waves with theoretically infinite long radiative lifetime, thus leading to a strong field localization. We here calculate the near E-field distributions in xy plane at $z = 60.5\,nm$. In Fig. 2(e), it is obvious that a giant near electric field enhancement over 200 times when a small tilting angle $\theta = 0.2°$ is introduced. With the increase of incident angle, field localization decreases gradually corresponding to a lower Q-factor, as shown in Fig. 2(f).

To move further ahead in the comprehension of the at-Γ BIC, breaking the structural symmetry of the resonator itself is an efficient pathway to couple the bound state to the normal incidence. Thus, the spacing between the resonators (g_1) is increased by moving the ring with the distance of Δ_x to break the in-plane mirror symmetry. Fig. 3(a) and 3(b) show that the EIT window would become more conspicuous if the displacement of the ring increases. The displacement mainly influences the coupling strength between the ring and its two nearest neighbour bars. When $\Delta_x = 0$, the bright mode cannot induce the dark-mode resonance due to symmetry incompatibility. As Δ_x increases, for instance, the coupling strength with the right bar is higher than that with the left bar, leading to the breaking of symmetry protection. The magnetic dipole with high-Q-factor resonance is excited by the coupling from rectangular bars, and then couples with the electric dipole moment destructively. As a result, a typical EIT can be obtained. To further unveil the BIC nature of such EIT effect, the radiative Q-factor as a function of in-plane symmetry breaking is demonstrated in Fig. 3(c). It is interesting to note that the Q-factor has the α^{-2} dependence (α is the asymmetry parameter defined as Δ_x/g_1), directly manifesting the validation of α^{-2} law [5]. To move further ahead in the distinguishment of physical mechanisms between tilting angle and displacement induced EIT/quasi-BIC, the E-field distributions at various Δ_x are displayed in Fig. 3(d)–3(f). This observation unequivocally shows that the near-field enhancement is more obvious when the displacement is smaller. However,
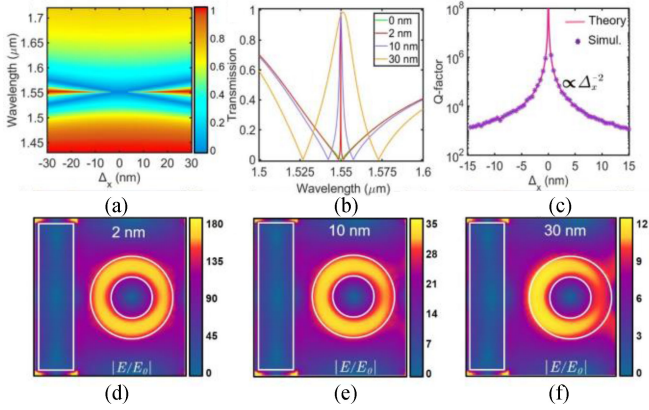
Fig. 3.   (a) Calculated transmission spectra of the collective dark and bright modes in the wavelength ranging from 1.43 μm to 1.72 μm and in the offset (Δ_x) ranging from -30 nm to 30 nm. A positive number moves to the right of the ring, while a negative number moves the opposite. (b) Calculated transmission spectra of the collective dark and bright modes in the wavelength ranging from 1.5 μm to 1.6 μm when the selected displacements (Δ_x) are 0 nm, 2 nm, 10 nm and 30 nm, respectively. (c) Variation of Q-factor of the collective dark and bright modes with varying incident offset (Δ_x). (d)-(f) Near-filed distributions at the function of offset (Δ_x) at the x-y cross section at z = 60.5 nm when the corresponding wavelength is 1.55 μm.
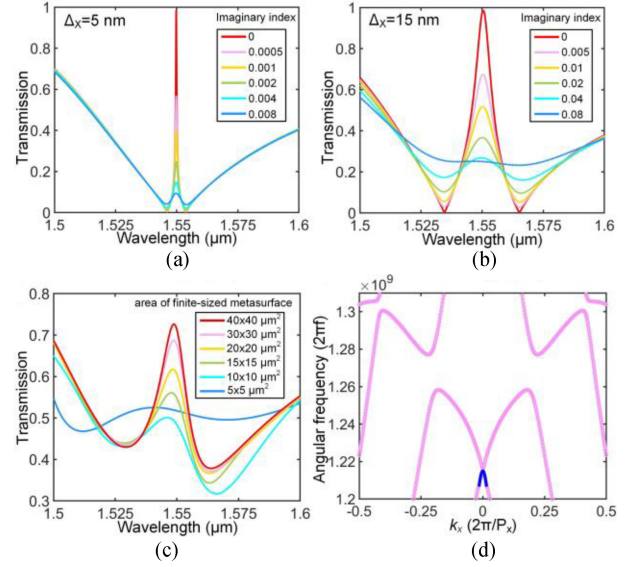

Fig. 4.   The quasi-BIC spectra evolution as a function of the loss of silicon material. (a) The spectra response by varying the imaginary part of silicon in the case with $\Delta_x = 5$ nm. (b) The spectra response by varying the imaginary part of silicon in the case with $\Delta_x = 15$ nm. (c) The quasi-BIC spectral evolution as a function of the size of the metasurface array. (d) Resonant modes calculated by the eigenmode analysis. The purple circles and blue curve represent the resonant eigenfrequencies and fitted quadratic function, respectively.

starkly contrasting with that of the tilting angle case, the E-field intensity distributes unevenly in the ring. Such phenomenon is clearly visible in Fig. 2(f) and 3(f), which is indicative of drastically different physical mechanisms behind. Indeed, incident angle tilting can directly 'lighten' the 'dark' mode by incoming wave, but the displacement causes the indirectly excitation from 'bright' mode. The indirection excitation would be influenced by the coupling coefficients, and different coupling strengths from left and right can naturally result in unsymmetric E-field distribution. Indeed, the tilting of incident wave can excite the magnetic resonance of the silicon ring with an extremely narrow linewidth, as shown in Fig. 1(d). When the rectangular bar with an obvious electric dipole resonance is introduced, two eigenmodes would unavoidably interact with each other and thus EIT is generated. Such a physical picture is not appliable to the case when the displacement of rectangular bar is carried out and the structure is illuminated by the normal incidence. In this case, the silicon ring holds a totally 'dark' mode and can only be excited by the near-field coupling from the rectangular bar. Such an indirection excitation would be influenced by the coupling coefficients, and different coupling strengths from left and right can naturally result in unsymmetric E-field distribution as shown in Fig. 3(f). As a result, if we define $|1 >$ and $|2 >$ as the eigenmodes of the rectangular bar and ring, respectively, the physical pictures for both cases can be depicted as follows. The EIT from tilting angle is a destructive interaction between $|1 >$ and $|2 >$, while the EIT from ring displacement is a destructive interference between $|1 >$ and $|1 > \rightarrow |2 > \rightarrow |3 >$.

The variation of loss in the silicon material can be considered as a good way to investigate the Q-damping effect. Here, the loss in the silicon is introduced by adding the imaginary part of refractive index during the simulations. As two representative examples, the spectra of $\Delta_x = 5\,nm$ and $\Delta_x = 15\,nm$ are used to represent the high-Q and low-Q quasi-BIC states, respectively.

Please note the disappearance of the EIT window here denotes the suppression of quasi-BIC. It is clearly seen from Fig. 4(a) and 4(b) that the high-Q based quasi-BIC is much more sensitive to the losses when compared with the low-Q one. It can thus be safely concluded that it is more challengeable to realize a quasi-BIC state with a higher Q factor in experiments. Furthermore, the spectra would unavoidably be influenced by the array size. It is clearly observed that the EIT window (quasi-BIC state) can be more obvious when the array size increases, as shown in Fig. 4(c). According to this tendency, the sharp resonance would be more conspicuous when the array size further increases. The resonance strength of quasi-BIC would increase when the size tends to infinity. The quasi-BIC resonance would disappear when the size is too small. Thus, we must fabricate a large area of the proposed metasurface to make sure a very high-Q resonance. Notably, the simulated tendency is very similar to the experimental observation in the [66]. Another factor to influence the Q-factor of quasi-BICs is the source dispersion effect since Gaussian beam with a characteristic spread in wave vector of k will excite a characteristic spread of frequencies $\Delta\omega = b\Delta k^2$. We thus calculate the eigenfrequencies as shown in Fig. 4(d). According to the Taylor expansion around the Γ point $\omega_{res}(k) = \omega_0 + bk^2$, we can then fit the dispersion of energy band to obtain the coefficient b as 0.0002 ω_0. As a result, the Q value is constrained by $Q \leq \omega_0/b\Delta k^2$. Based on the results in the [73], the maximal Q-factor is moderately high $Q \approx 5 \times 10^3$ when a Gaussian beam with a waist radius of 7 μm excite the metasurface.

Such a silicon-based metasurfaces can be fabricated through mature techniques [66]. First, the silicon layer can be simply
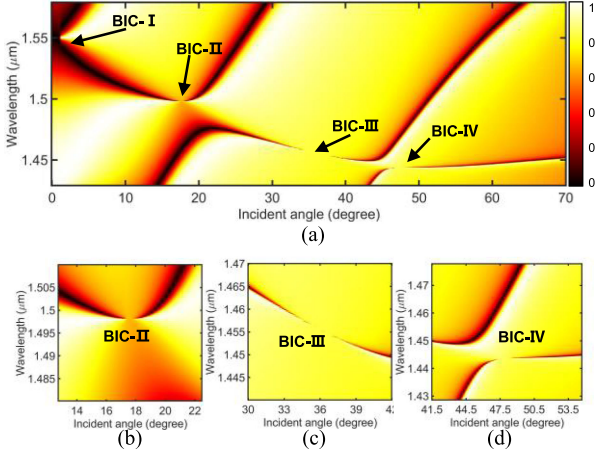
Fig. 5. (a) Calculated transmission spectra of the coupled resonators in the wavelength ranging from 1.43 μm to 1.52 μm and in the incident angle ranging from 0° to 70°. (b)-(d) The detailed spectral mappings of three off-Γ BICs marked as BIC-II, the BIC-III and the BIC-IV, respectively.
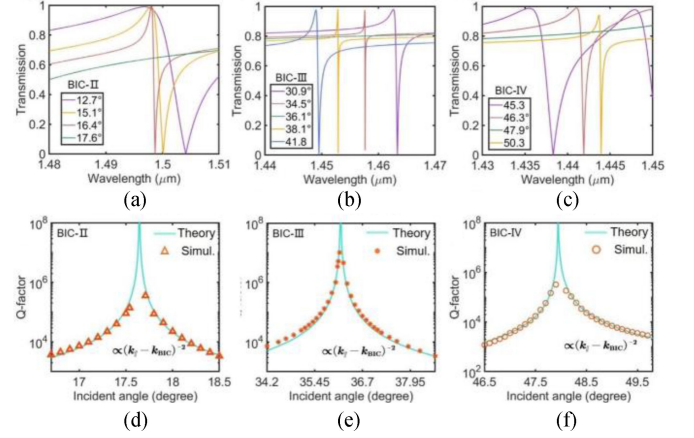

Fig. 6. (a)-(c) Calculated transmission spectra of the BIC-II, BIC-III and BIC-IV respectively with various incident angles close to the BIC points. (d)-(f) Variation of Q-factor of the BIC-II, BIC-III and BIC-IV respectively.

deposited on a quartz wafer by means of chemical vapor deposition. Then, the technique of electron beam lithography (EBL) can be used to define the metasurface pattern on the silicon layer. Final, the metasurfaces can be created by the lift-off process and reactive ion beam etching (RIE). Since the planar structure is used in our work, the fabrication can be carried out without much difficulty. However, there also exists some fabrication constraints when it comes into realizing high-Q EIT resonances by geometry symmetry breaking. Because the tiny displacement of the rectangular bar plays an important role in the success of high-Q EIT resonance, the fabrication process should be accurate enough.

B. Accidental BICs at Off-Γ Points

Besides the symmetry-protected BIC, accidental BICs resulted from an avoidable crossing of different eigenstates via geometric or angle detuning are ubiquitous in photonics slabs. The vanishing of one of the crossing modes is characterized by the Fredrich–Wintegen (FW) scenario [4]. These off-Γ BIC in our proposed system can also be obtained by monitoring the mode hybridization at the wave vector. The existence of off-Γ BIC is the signature of strong coupling, whose requirement can be obtained by using coupled mode theory in two modes and two ports. The Hamiltonian is:

$$H = \begin{bmatrix} \omega_a & \kappa \\ \kappa & \omega_b \end{bmatrix} - i \begin{bmatrix} \gamma_a & \sqrt{\gamma_a \gamma_b e^{i\phi}} \\ \sqrt{\gamma_a \gamma_b} e^{i\phi} & \gamma_b \end{bmatrix} \quad (1)$$

where ω_a and ω_b are the eigenfrequencies of two modes, respectively. γ is the radiative loss. κ is the coupling strength between two modes. $\phi = 0$ due to the in-plane coupling studied here. If one of the coupled eigenmodes become purely real without any loss, the following condition is satisfied:

$$(\omega_a - \omega_b) = \sqrt{\gamma_a \gamma_b} (\gamma_a - \gamma_b) \quad (2)$$

As shown in Fig. 5(a), several off-Γ BICs, marked as BIC-II, BIC-III and BIC-IV, are found in the incident angle range

varying from 0° to 70°. Compared with the results shown in Fig. 1(c), a new energy band that blueshifts monotonously with the incident angle increasing is formed when the two resonators are coupled. This band would cross with other bands at different incident angles, indicating the hybridizations of two modes. In Fig. 5(b)–(d), it is obvious that transmission resonance linewidths disappear when the incident angle reaches 17.6°, 36.1°, and 47.9°, respectively. In these BICs, the anti-crossing phenomenon in BIC-II and BIC-IV is conspicuous, in which the blueshift band collides with the redshift ones. As a result, BIC-II and IV are FW BICs. However, BIC-III possesses a faint transmission resonance line without the coupling from two modes but a single resonance evolves into a non-radiative mode. The concept of single-resonance parametric BIC was first proposed in the [38]. Unlike the symmetry-incompatibility and interaction between two resonances, the single-resonance parametric BIC can only occur at the off-Γ point when one resonance exists. The physical picture behind it can be depicted as follows: The field profile inside the dielectric metasurface could be considered as a superposition of waves with different propagation constants. At the interfaces, the wave partly reflects back into the metasurface, and partly becomes an outgoing plane wave. At appropriate off-Γ points, the formation of a BIC point is resulted from interference of the transmitted waves with different propagation constants. Please note that these 'accidental' crossings at off-Γ points are distinct from symmetry-protected BIC-I in which leakage channel is forbidden owing to the 'dark' nature of the ring.

Regarding the resonance lifetime near these off-Γ BICs, spectral features and Q-factor evolutions about the sharp resonance features are shown in Fig. 6. The spectral profiles show transmission dips with a typical asymmetric Fano feature. For BIC-II, Fig. 6(a) shows that the linewidth at incident angle 17.6° disappears, indicating no leakage of energy. When the incident angle deviates 17.6°, we can see that there is an obvious width broadening of these transmission dips, namely, the occurrence of quasi-BIC. For BIC-III, Fig. 6(b) shows BIC occurs at the incident angle of 36.1° and quasi-BICs occur with Fano-shape dips by slightly tuning the incident angle. For BIC-IV, Fig. 6(c)

TABLE I
PHYSICAL PARAMETER

BIC	Physical parameter	Value
BIC-II (15.1°)	γ_1	1.0642 THz
	γ_2	2.6394 THz
	κ	2.4336 THz
	$\omega_1/2\pi$	200.6995 THz
	$\omega_2/2\pi$	208.1000 THz
BIC-II (16.4°)	γ_1	0.3422 THz
	γ_2	3.1637 THz
	κ	1.0465 THz
	$\omega_1/2\pi$	200.3453 THz
	$\omega_2/2\pi$	207.0000 THz
BIC-IV (45.3°)	γ_1	0.0312 THz
	γ_2	0.6539 THz
	κ	0.3250 THz
	$\omega_1/2\pi$	208.0603 THz
	$\omega_2/2\pi$	206.4144 THz
BIC-IV (46.3°)	γ_1	0.0025 THz
	γ_2	0.75 THz
	κ	0.1607 THz
	$\omega_1/2\pi$	207.8686 THz
	$\omega_2/2\pi$	205.4517 THz

Fig. 7. (a)-(j) Near E-field distributions at the Fano dips with different incident light angles. The sections are all fixed in the xy plane at z = 60.5 nm within one unit-cell.

clearly demonstrates that the BIC occurs at the 47.9° incident angle, and at other incident angles, such as 45.3°, 46.3° and 50.3°, quasi-BIC occurs. Moreover, the corresponding Q-factors as a function incident angle are shown in Fig. 6(d)–(e) and 6(f) respectively. The Q-factors near these three BICs can reach up to more than 10^5. The theoretical curves are all fitted by the formula $|\alpha|\kappa \sin\theta - \kappa \sin\theta_{\mathrm{BIC}}|^{-2}$, where θ_{BIC} is the incident angle that BIC occurs [37]. The calculated data manifests that the numerical results are in good agreement with the theoretical curves. Thus, such infinite high-Q points can be identified as off-Γ BICs. Besides, we try to fit the transmission amplitude of the quasi-BICs of II and IV according the formula derived from [74]. The detailed deviation process is provided in the supplemental information. The fitted key parameters are shown in Table I, in which the coupling of two resonances is solidly observed and the quasi-BIC states possess an extremely low radiative loss.

To further unveil the underneath mechanisms of these BICs, the near E-field distributions pertaining to the off-Γ BICs are investigated in the *xy*-plane at z = 60.5 nm as well. Fig. 7(a)–(c) display the E-field distributions at the incident angles near BIC-II and the frequency of each Fano dip. Fig. 7(d)–(f) are correspond to the BIC-III case and Fig. 7(h)–(j) correspond to the BIC-III case. It is easy to discern that the E-fields in Fig. 7(a)–(d) and 7(h) are relatively low when compared with the quasi-BIC cases. This is mainly attributed to the decoupling between the incoming wave and the eigenmode owing to the destructive interference between two modes. It is intriguing that the local field enhancement of BIC-II occurs mainly in the electric dipole gap, which is 6 times higher than the incident field. The reason behind can be seen in Fig. 5(a) and 5(b), in which the BIC-II point locates near the band from the resonance of the rectangular bar. As a result, the resonance of the ring is highly suppressed by leaving the electric dipole with high radiative loss alive. However, such balance is broken with little incident angle variation when the mode of the
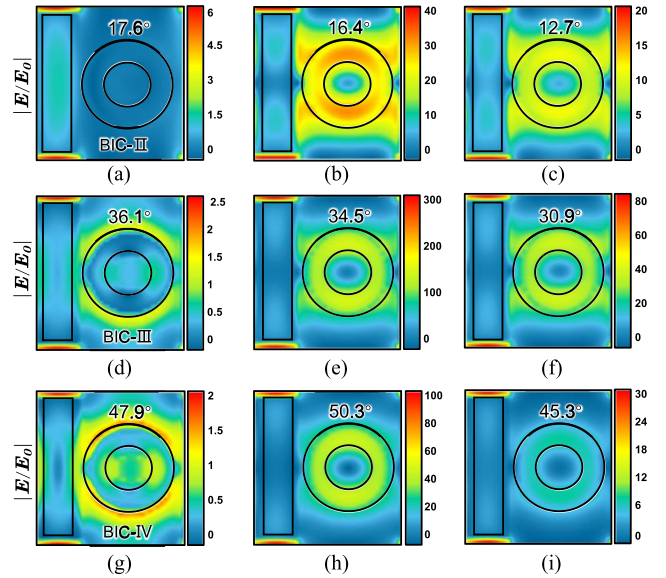
ring starts to radiate with ultralong lifetime, as shown in Fig. 7(b) and 7(c). As for the quasi-BICs shown in Fig. 7(e) and 7(f), the near-fields exhibit an almost the same profile no matter whether how extent the angle deviates the critical angle. This result is inevitably relevant to the configuration of single-resonance parametric BIC since BIC-III exists in the band where only one resonant mode evolutes. For the quasi-BICs close to BIC-IV, the situation is a little different. As abovementioned, BIC-IV is formed due to the avoided crossing between two energy bands in the photonic crystal slab. In Fig. 4(d), we can see that the anti-crossing behaviour takes place at the left of the BIC point. Thus, the quasi-BIC states at the incident angle less than 47.9° would be influenced from the redshift band strongly, while the states at the incident angle higher than 47.9° would maintain the resonant state of the blueshift band. The idea can be evident from the E-field distributions in Fig. 7(h) and 7(i). Consistent with the generation mechanism outlined above when the incident angle is 45.3°, the E-field enhancement primarily originates from the rectangular bar, which possesses the resonant feature of the redshift band. Nevertheless, the E-field at 50.3° exhibits a similar distribution when compared with the cases shown in Fig. 7(e) and 7(f). Therefore, it is gratifying to see that the near-field coupling from two individual resonator is a very effective approach to construct multiple BICs by energy band anti-crossing effects.

III. CONCLUSION

In summary, we have systematically investigated the BIC nature in a coupled mode photon cavity comprising a rectangular bar and a ring within one unit-cell. Our results manifest the existence of multiple BICs which are formed by the coupling effect between the two resonators. According to the physical mechanism, they are classified as a symmetry-protected at-Γ

BIC and three off-Γ BICs. For the at-Γ BIC, we have found that it holds an intrinsic connection with the well-studied EIT effect which is generated when the at-Γ BIC evolves into quasi-BIC state. Intriguingly, the EIT window formed by a slight angle tilting is due to the 'bright-bright' mode coupling, while the EIT window induced by displacement of resonator is owing to the 'bright-dark' mode coupling. For off-Γ BICs, they are created when the incident angles are 17.6°, 36.1° or 47.9°, respectively. Two of them are ascribed to the avoided crossings with two energy bands and another one belongs to the single-resonance parametric BIC. Besides, the Q-factors of all quasi-BICs are extremely high and can reach up to 10^5. The Q-factor evolution of each individual BIC accords well with the theoretical α^{-2} law. Therefore, the coupled resonators in photonic slabs not only provide a unique degree of freedom to manipulate abundant BIC-based resonances, but also bear a high potential for various photonics applications, such as ultranarrow-band filters, slow-light devices, ultrasensitive sensors, and ultraefficient modulators.

REFERENCES

[1] D. C. Marinica, A. G. Borisov, and S. V. Shabanov, "Bound states in the continuum in photonics," *Phys. Rev. Lett.,* vol. 100, no. 18, May 2008, Art. no. 183902.

[2] C. W. Hsu, B. Zhen, A. D. Stone, J. D. Joannopoulos, and M. Soljačić, "Bound states in the continuum," *Nature Rev. Mater.,* vol. 1, no. 9, Jul. 2016, Art. no. 16048.

[3] J. Von Neumann and E. Wigner, "Über merkwürdige diskrete eigenwerte phys," *Physikalische Zeitschrift,* vol. 30, no. 524, pp. 465–467, 1929.

[4] H. Friedrich and D. Wintgen, "Interfering resonances and bound states in the continuum," *Phys. Rev. A,* vol. 32, no. 6, pp. 3231–3242, Dec. 1985.

[5] K. Koshelev, S. Lepeshov, M. Liu, A. Bogdanov, and Y. Kivshar, "Asymmetric metasurfaces with high-Q resonances governed by bound states in the continuum," *Phys. Rev. Lett.,* vol. 121, no. 19, Nov. 2018, Art. no. 193903.

[6] B. Wang *et al.*, "Generating optical vortex beams by momentum-space polarization vortices centred at bound states in the continuum," *Nature Photon.,* vol. 14, no. 10, pp. 623–628, 2020.

[7] Z. Zhang, J. Yang, T. Du, H. Ma, and X. Jiang, "Tailoring bound states in the continuum in symmetric photonic crystal slabs by coupling strengths," *Opt. Exp.,* vol. 30, no. 5, pp. 8049–8062, Feb. 2022.

[8] T. Shi *et al.*, "Planar chiral metasurfaces with maximal tunable chiroptical response driven by bound states in the continuum," 2021, *arXiv:2112.07122.*

[9] A. Overvig, N. Yu, and A. Alù, "Chiral quasi-bound states in the continuum," *Phys. Rev. Lett.,* vol. 126, no. 7, 2021, Art. no. 073001.

[10] W. Liu *et al.*, "Circularly polarized states spawning from bound states in the continuum," *Phys. Rev. Lett.,* vol. 123, no. 11, 2019, Art. no. 116104.

[11] D. Shen, X. Ren, Q. Ci, K. Niu, S. Wang, and Z. Huang, "Dual quasi-bound states in the continuum modes for optical activity manipulation," *IEEE Photon. J.,* vol. 13, no. 6, Dec. 2021, Art no. 4600105.

[12] C. Huang *et al.*, "Ultrafast control of vortex microlasers," *Science,* vol. 367, no. 6481, pp. 1018–1021, Feb. 2020.

[13] Y. Yu, A. Sakanas, A. R. Zali, E. Semenova, K. Yvind, and J. Mørk, "Ultra-coherent Fano laser based on a bound state in the continuum," *Nature Photon.,* vol. 15, no. 10, pp. 758–764, Oct. 2021.

[14] M.-S. Hwang *et al.*, "Ultralow-threshold laser using super-bound states in the continuum," *Nature Commun.,* vol. 12, no. 1, Jul. 2021, Art. no. 4135.

[15] Z. Zheng, Y. Zhu, J. Duan, M. Qin, F. Wu, and S. Xiao, "Enhancing Goos-Hänchen shift based on magnetic dipole quasi-bound states in the continuum in all-dielectric metasurfaces," *Opt. Exp.,* vol. 29, no. 18, pp. 29541–29549, Aug. 2021.

[16] J. Wang *et al.*, "Shifting beams at normal incidence via controlling momentum-space geometric phases," *Nature Commun.,* vol. 12, no. 1, Oct. 2021, Art. no. 6046.

[17] L. Vertchenko, C. DeVault, R. Malureanu, E. Mazur, and A. Lavrinenko, "Near-zero index photonic crystals with directive bound states in the continuum," *Laser Photon. Rev.,* vol. 15, no. 7, 2021, Art. no. 2000559.

[18] C. Fang *et al.*, "Efficient second-harmonic generation from silicon slotted nanocubes with bound states in the continuum," *Laser Photon. Rev.,* vol. 16, no. 5, May 2022, Art. no. 2100498.

[19] L. Carletti, K. Koshelev, C. De Angelis, and Y. Kivshar, "Giant nonlinear response at the nanoscale driven by bound states in the continuum," *Phys. Rev. Lett.,* vol. 121, no. 3, 2018, Art. no. 033903.

[20] H. K. Gandhi, D. Rocco, L. Carletti, and C. De Angelis, "Gain-loss engineering of bound states in the continuum for enhanced nonlinear response in dielectric nanocavities," *Opt. Exp.,* vol. 28, no. 3, pp. 3009–3016, Feb. 2020.

[21] Z. Liu *et al.*, "High-Q quasibound states in the continuum for nonlinear metasurfaces," *Phys. Rev. Lett.,* vol. 123, no. 25, 2019, Art. no. 253901.

[22] Q. Yang, Y. Liu, X. Gan, C. Fang, G. Han, and Y. Hao, "Nonlinear bound states in the continuum of etchless lithium niobate metasurfaces," *IEEE Photon. J.,* vol. 12, no. 5, Oct. 2020, Art. no. 4601209.

[23] T. C. Tan *et al.*, "Active control of nanodielectric-induced THz quasi-BIC in flexible metasurfaces: A platform for modulation and sensing," *Adv. Mater.,* vol. 33, no. 27, Jul. 2021, Art. no. 2100836.

[24] S. Han *et al.*, "All-dielectric active terahertz photonics driven by bound states in the continuum," *Adv. Mater.,* vol. 31, no. 37, 2019, Art. no. 1901921.

[25] Y. Wang, Z. Han, Y. Du, and J. Qin, "Ultrasensitive terahertz sensing with high-Q toroidal dipole resonance governed by bound states in the continuum in all-dielectric metasurface," *Nanophotonics,* vol. 10, no. 4, pp. 1295–1307, 2021.

[26] J. Lee *et al.*, "Observation and differentiation of unique high-Q optical resonances near zero wave vector in macroscopic photonic crystal slabs," *Phys. Rev. Lett.,* vol. 109, no. 6, 2012, Art. no. 067401.

[27] C. W. Hsu, B. Zhen, S.-L. Chua, S. G. Johnson, J. D. Joannopoulos, and M. Soljačić, "Bloch surface eigenstates within the radiation continuum," *Light: Sci. Appl.,* vol. 2, no. 7, Jul. 2013, Art. no. e84.

[28] Y. Yang, C. Peng, Y. Liang, Z. Li, and S. Noda, "Analytical perspective for bound states in the continuum in photonic crystal slabs," *Phys. Rev. Lett.,* vol. 113, no. 3, 2014, Art. no. 037401.

[29] X. Zhao *et al.*, "Terahertz investigation of bound states in the continuum of metallic metasurfaces," *Optica,* vol. 7, no. 11, pp. 1548–1554, 2020.

[30] J. Niu, Y. Zhai, Q. Han, J. Liu, and B. Yang, "Resonance-trapped bound states in the continuum in metallic THz metasurfaces," *Opt. Lett.,* vol. 46, no. 2, pp. 162–165, 2021.

[31] L. Liang, Q. Zheng, X. Nan, and Y. Dong, "Asymmetric all-dielectric active metasurface for efficient dual reflection modulation," *Opt. Commun.,* vol. 505, Feb. 2022, Art. no. 127539.

[32] Z. Li, Q. Zhu, Y. Wang, and S. Xie, "Bound states in the continuum in the double-period rectangular hole arrays perforated in one layer of photonic crystal slab in the visible wavelength region," *Opt. Commun.,* vol. 436, pp. 151–160, Apr. 2019.

[33] Y. Liang *et al.*, "Bound states in the continuum in anisotropic plasmonic metasurfaces," *Nano Lett.,* vol. 20, no. 9, pp. 6351–6356, Sep. 2020.

[34] Q. Zhou *et al.*, "Geometry symmetry-free and higher-order optical bound states in the continuum," *Nature Commun.,* vol. 12, no. 1, Jul. 2021, Art. no. 4390.

[35] M. Liu and D.-Y. Choi, "Extreme Huygens' metasurfaces based on quasi-bound states in the continuum," *Nano Lett.,* vol. 18, no. 12, pp. 8062–8069, Dec. 2018.

[36] I. Kuznetsov Arseniy, E. Miroshnichenko Andrey, L. Brongersma Mark, S. Kivshar Yuri, and B. Luk'yanchuk, "Optically resonant dielectric nanostructures," *Science,* vol. 354, no. 6314, Nov. 2016, Art. no. aag2472.

[37] S. Han, P. Pitchappa, W. Wang, Y. K. Srivastava, M. V. Rybin, and R. Singh, "Extended bound states in the continuum with symmetry-broken terahertz dielectric metasurfaces," *Adv. Opt. Mater.,* vol. 9, no. 7, 2021, Art. no. 2002001.

[38] C. W. Hsu *et al.*, "Observation of trapped light within the radiation continuum," *Nature,* vol. 499, no. 7457, pp. 188–191, 2013.

[39] J. D. Joannopoulos, S. G. Johnson, J. N. Winn, and R. D. Meade, *Photonic Crystals: Molding the Flow of Light*, 2nd ed., Princeton, NJ, USA: Princeton Univ. Press, 2011.

[40] X. Gao *et al.*, "Formation mechanism of guided resonances and bound states in the continuum in photonic crystal slabs," *Sci. Rep.*, vol. 6, no. 1, Aug. 2016, Art. no. 31908.

[41] A. I. Ovcharenko, C. Blanchard, J.-P. Hugonin, and C. Sauvan, "Bound states in the continuum in symmetric and asymmetric photonic crystal slabs," *Phys. Rev. B,* vol. 101, no. 15, Apr. 2020, Art. no. 155303.

[42] B. Zhen, C. W. Hsu, L. Lu, A. D. Stone, and M. Soljačić, "Topological nature of optical bound states in the continuum," *Phys. Rev. Lett.,* vol. 113, no. 25, Dec. 2014, Art. no. 257401.

[43] Q. Shi, J. Zhao, and L. Liang, "Two dimensional photonic crystal slab biosensors using label free refractometric sensing schemes: A review," *Prog. Quantum Electron.*, vol. 77, May 2021, Art. no. 100298.

[44] A. Tavousi, M. R. Rakhshani, and M. A. Mansouri-Birjandi, "High sensitivity label-free refractometer based biosensor applicable to glycated hemoglobin detection in human blood using all-circular photonic crystal ring resonators," *Opt. Commun.*, vol. 429, pp. 166–174, Dec. 2018.

[45] M. L. Tseng, Y. Jahani, A. Leitis, and H. Altug, "Dielectric metasurfaces enabling advanced optical biosensors," *ACS Photon.*, vol. 8, no. 1, pp. 47–60, Jan. 2021.

[46] D. C. Zografopoulos and V. Dmitriev, "Quasi-dark resonances in silicon metasurface for refractometric sensing and tunable notch filtering," *J. Lightw. Technol.*, vol. 39, no. 21, pp. 6985–6993, Nov. 2021.

[47] Y. Guo, M. Xiao, Y. Zhou, and S. Fan, "Arbitrary polarization conversion with a photonic crystal slab," *Adv. Opt. Mater.*, vol. 7, no. 14, Jul. 2019, Art. no. 1801453.

[48] W. Ye, Y. Gao, and J. Liu, "Singular points of polarizations in the momentum space of photonic crystal slabs," *Phys. Rev. Lett.*, vol. 124, no. 15, Apr. 2020, Art. no. 153904.

[49] X. Chen, Y. Zhou, X. Ma, W. Fang, W. Zhang, and W. Gao, "Polarization conversion in anisotropic dielectric metasurfaces originating from bound states in the continuum," *Opt. Lett.*, vol. 46, no. 17, pp. 4120–4123, Sep. 2021.

[50] S. Han *et al.*, "All-dielectric active terahertz photonics driven by bound states in the continuum," *Adv. Mater.*, vol. 31, no. 37, Sep. 2019, Art. no. 1901921.

[51] Z. Wang, L. Chen, X. Li, T. Lang, X. Jing, and Z. Hong, "Analogue of electromagnetically-induced transparency with ultra-narrow bandwidth in a silicon terahertz metasurface," *Opt. Mater. Exp.*, vol. 11, no. 7, pp. 1943–1952, Jul. 2021.

[52] D. R. Abujetas, Á. Barreda, F. Moreno, A. Litman, J.-M. Geffrin, and J. A. Sánchez-Gil, "High-Q transparency band in all-dielectric metasurfaces induced by a Quasi bound state in the continuum," *Laser Photon. Rev.*, vol. 15, no. 1, Jan. 2021, Art. no. 2000263.

[53] C. Kyaw *et al.*, "Polarization-selective modulation of supercavity resonances originating from bound states in the continuum," *Commun. Phys.*, vol. 3, no. 1, Nov. 2020, Art. no. 212.

[54] J. F. Algorri *et al.*, "Strongly resonant silicon slot metasurfaces with symmetry-protected bound states in the continuum," *Opt. Exp.*, vol. 29, no. 7, pp. 10374–10385, Mar. 2021.

[55] Y. K. Srivastava, R. T. Ako, M. Gupta, M. Bhaskaran, S. Sriram, and R. Singh, "Terahertz sensing of 7 nm dielectric film with bound states in the continuum metasurfaces," *Appl. Phys. Lett.*, vol. 115, no. 15, Oct. 2019, Art. no. 151105.

[56] S. Romano *et al.*, "Tuning the exponential sensitivity of a bound-state-in-continuum optical sensor," *Opt. Exp.*, vol. 27, no. 13, pp. 18776–18786, Jun. 2019.

[57] J. F. Algorri, D. C. Zografopoulos, A. Ferraro, B. García-Cámara, R. Beccherelli, and J. M. Sánchez-Pena, "Ultrahigh-quality factor resonant dielectric metasurfaces based on hollow nanocuboids," *Opt. Exp.*, vol. 27, no. 5, pp. 6320–6330, Mar. 2019.

[58] N. Papasimakis, V. A. Fedotov, N. I. Zheludev, and S. L. Prosvirnin, "Metamaterial analog of electromagnetically induced transparency," *Phys. Rev. Lett.*, vol. 101, no. 25, Dec. 2008, Art. no. 253903.

[59] M. D. Lukin and A. Imamoğlu, "Controlling photons using electromagnetically induced transparency," *Nature*, vol. 413, no. 6853, pp. 273–276, Sep. 2001.

[60] C. Hu, S. A. Schulz, A. A. Liles, and L. O'Faolain, "Tunable optical buffer through an analogue to electromagnetically induced transparency in coupled photonic crystal cavities," *ACS Photon.*, vol. 5, no. 5, pp. 1827–1832, May 2018.

[61] Z.-G. Dong *et al.*, "Enhanced sensing performance by the plasmonic analog of electromagnetically induced transparency in active metamaterials," *Appl. Phys. Lett.*, vol. 97, no. 11, 2010, Art. no. 114101.

[62] J. Gu *et al.*, "Active control of electromagnetically induced transparency analogue in terahertz metamaterials," *Nature Commun.*, vol. 3, no. 1, pp. 1–6, 2012.

[63] J. F. Algorri *et al.*, "Analogue of electromagnetically induced transparency in square slotted silicon metasurfaces supporting bound states in the continuum," *Opt. Exp.*, vol. 30, no. 3, pp. 4615–4630, Jan. 2022.

[64] W. Shi *et al.*, "Terahertz bound states in the continuum with incident angle robustness induced by a dual period metagrating," *Photon. Res.*, vol. 10, no. 3, pp. 810–819, Mar. 2022.

[65] L. Cong and R. Singh, "Symmetry-protected dual bound states in the continuum in metamaterials," *Adv. Opt. Mater.*, vol. 7, no. 13, Jul. 2019, Art. no. 1900383.

[66] Y. Yang, I. I. Kravchenko, D. P. Briggs, and J. Valentine, "All-dielectric metasurface analogue of electromagnetically induced transparency," *Nature Commun.*, vol. 5, no. 1, Dec. 2014, Art. no. 5753.

[67] Y. Yang *et al.*, "Nonlinear Fano-resonant dielectric metasurfaces," *Nano Lett.*, vol. 15, no. 11, pp. 7388–7393, 2015.

[68] Z. F. Sadrieva *et al.*, "Transition from optical bound states in the continuum to leaky resonances: Role of substrate and roughness," *ACS Photon.*, vol. 4, no. 4, pp. 723–727, Apr. 2017.

[69] D. V. Evans and R. Porter, "On the existence of embedded surface waves along arrays of parallel plates," *Quart. J. Mechanics Appl. Math.*, vol. 55, no. 3, pp. 481–494, 2002.

[70] E. N. Bulgakov and A. F. Sadreev, "Bloch bound states in the radiation continuum in a periodic array of dielectric rods," *Phys. Rev. A*, vol. 90, no. 5, Nov. 2014, Art. no. 053801.

[71] E. N. Bulgakov and A. F. Sadreev, "Light trapping above the light cone in a one-dimensional array of dielectric spheres," *Phys. Rev. A*, vol. 92, no. 2, Aug. 2015, Art. no. 023816.

[72] S. Longhi and G. D. Valle, "Floquet bound states in the continuum," *Sci. Rep.*, vol. 3, no. 1, Jul. 2013, Art. no. 2219.

[73] A. C. Overvig, S. C. Malek, M. J. Carter, S. Shrestha, and N. Yu, "Selection rules for quasibound states in the continuum," *Phys. Rev. B*, vol. 102, no. 3, Jul. 2020, Art. no. 035434.

[74] W. Huang *et al.*, "A complete phase diagram for dark-bright coupled plasmonic systems: Applicability of Fano's formula," *Nanophotonics*, vol. 9, no. 10, pp. 3251–3262, 2020.